Fluidization and Fluid Particle Systems

Recent Research and Development

Fluidization and Fluid Particle Systems: Recent Research and Development

Hamid Arastoopour, *Volume Editor*

John C. Chen, Ye Mon Chen, Leon Glicksman, Desmond King, and Wen-Ching Yang, *Volume Co-Editors*

Mengtian Bai
Bernard Barry
J. Baxter
Chia-Min Chen
Wei-Yin Chen
N. Choueau
Clive E. Davies
S. Faderani
L.T. Fan
Leon R. Glicksman
P. Guigon.
H. Hatano
D.M. Heyes
B.P.B. Hoomans
Matthew R. Hyre
J.H. Kim
J.A.M. Kuipers
Mooson Kwauk
J. -F. Large
Lii-Ping Leu
T. Masuyama
S. Sakurai
Jaap C. Schouten
K. Shakourzadeh
D.L.O. Smith
Madhava Syamlal
H. Takeuchi
Stephen Tallon
R.B.Thorpe
K. Tsuchiya
U. Tüzün
Cor M. van den Bleek
John van der Schaaf
W. P. M. van Swaaij

AIChE Staff
Maura N. Mullen, Managing Editor
Armand Veneziano, Cover Design

AIChE Symposium Series

Number 318 | 1998 | Volume 94

Published by

American Institute of Chemical Engineers

3 Park Avenue | New York, N.Y. 10016-5901

American Institute of Chemical Engineers (AIChE)
3 Park Avenue
New York, N.Y. 10016-5901
U.S.A.

AIChE shall not be responsible for statements or opinions advanced in their papers or printed in their publications.

Library of Congress Cataloging-in-Publication Data

Fluidization and fluid particle systems : recent research and development / Hamid Arastoopour, volume editor ; John C. Chen ... [et al.], volume co-editors.
p. cm. -- (AIChE symposium series, ISSN 0065-8812 ; no. 318, v. 94)
"Presented in twelve sessions at the AIChE Annual Meeting in Los Angeles, California, November 16, through 21, 1997" --
Includes index.
ISBN 0-8169-0774-9
1. Fluidization--Congresses. 1. Arastoopour, Hamid. II. Chen John C., 1934- . III. American Institute of Chemical Engineers. Meeting (1997 : Los Angeles, Calif.) IV. Series: AIChE symposium series ; no. 318.
TP156.F65F5736 1998
660'.284292--dc21 98-36294
CIP

FOREWORD

This volume of the AIChE Symposium Series continues the tradition of an annual volume presenting recent research and development in fluidization and fluid-particle systems. The papers were selected by peer reviews from those presented in twelve sessions at the AIChE Annual Meeting in Los Angeles, California, November 16 through 21, 1997.

This year's symposium volume contains papers that cover a wide range of topics related to fluid-particle systems and fluidization including:

- Fundamentals of Fluidization and Fluid-Particle Systems
- Particle Interaction
- Circulating Fluidized Bed
- Modeling and Computer Simulation of Fluid-Particle Systems
- Advances in Fluid-Particle Flow Measurements, Handling and Processing

The first article is a fluidization plenary paper entitled "Exploring the Multi-Phase Nature of Fluidization" by Professor Mooson Kwauk of the Institute of Chemical Metallurgy, Academia Sinica, China, who received the 1997 Fluidization Lectureship Award sponsored by Fluor Daniel Foundation.

I would like to acknowledge all the chairs and co-chairs of the sessions for their careful selection of papers for the Los Angeles meeting. I would also like to thank my co-editors, AIChE Managing Editor Maura N. Mullen, Dr. Amir Riahi, and the fluidization particle technology research team at Illinois Institute of Technology, whose critical review and further evaluation of the papers ensured the high quality of the papers in this volume. Finally, I would like to express my thanks to my assistant, Simone Bradford, without whose diligence, quality control and hard work, this volume would not have been possible.

Hamid Arastoopour, *Volume Editor*
Professor and Chairman
Department of Chemical and Environmental Engineering
Illinois Institute of Technology
10 W. 33rd Street
Chicago, Illinois 60616

CONTENTS

Plenary Paper

Exploring the Multi-Phase Nature of Fluidization

Mooson Kwauk
Institute of Chemical Metallurgy, Academia Sinica, Beijing 100080, China

When Fluidization was first studied in the 1940's, it was treated as a global phenomenon. People were concerned with primary variables, such as, the velocity at which particles start to fluidize and how much the solids bed expand with velocity, etc. When chemical reaction took place in a fluidized bed, it was treated in the manner of its kin, the fixed-bed reactor, in terms of yield, conversion, and other factors which obtain at the inlet and outlet of the fluidized bed. With intensification of application, however, we require more precise knowledge about the in situ heterogeneity of the fluidized systems and we need to know what actually happens to individual particles as they react with the gas. This presentation explores the following aspects of the multi-phase nature of fluidization:

Morphological Changes of Reacting Particles
Heterogeneity/Homogeneity in Particle-Fluid Two-Phase Flow
Improvement of G/L Conatacting with Fluidized Solids
Fluidization of Particles with Appreciable Inter-Particle Forces

When fluidization was first studied in the 1940's, it was treated as a global phenomenon, and people were concerned with such primary variables as the velocity at which particles start to fluidize, how much the solids bed expands with velocity, etc. When chemical reaction took place in a fluidized bed, it was once treated much in the manner of its kin, the fixed-bed reactor, in terms of yield, conversion, and other factors which obtain at the inlet and outlet of the fluidized bed. With intensification of application, however, we need more precise knowledge of the *in situ* heterogeneity of the fluidized systems and we need to know what actually happens to *individual* particles as they react with gas. I feel honored to be invited to share with you some of our in-house studies, which explore a few aspects of such multi-phase nature of fluidization.

MORPHOLOGICAL CHANGES OF REACTING PARTICLES (Z. Cao, M. Shao , X. Ma)

In the case of a reacting solid particle, it is often geometrically simplified to a sphere or a spherical agglomerate of smaller spheres. While the supposition of a sphere simplifies mathematical modeling, it fails to reflect what actually happens to the particle during processing. Two attempts were made to reveal the morphological changes of a reacting solid particle: observation of a reacting solid particle while it is acoustically levitated, and observation of the solid surface in a microreactor under a scanning electron microscope.

When a single particle is levitated in a flowing reacting medium, the whole reaction process of a given particle could be traced visually while eliminating interactions from other particles as well as from the reactor walls. Acoustic levitation is used in such containment of single particles in fluid media. To counteract the dependence of sound wave propagation on the changing properties of the fluid medium during the course of reaction, a resonance tracking function is required to compensate the effects due to medium changes in order to maintain stable levitation of the particles. Theoretical analysis showed that there are two factors which can be manipulated to maintain resonance in the chamber: the length L of the chamber and the frequency f of the sound wave.

Figure 1-1 shows the single-axis acoustic levitation reactor together with its resonance tracking system. A piezoceramic transducer operated at 20 kHz is used as the sound source. Phase shift between the input and output of the chamber is used as the measurement

multitude of minute nuclei of nascent oxide. Above this thin layer is a second, more or less compact layer consisting of agglomerated grains due to protracted residence, and above this intermediate layer is another layer of discrete younger grains, rectangular or hexagonal, stick-like or whiskers, according to reaction conditions, while Fe and O diffuse countercurrently to each other.

Mathematically, attempts were made to adapt existing methodology to modeling complex particle morphology, e.g., simplification of the Fourier analysis from cosine series, which employs both amplitude coefficients and phase angles, to pure sine series (**Figure 1-9**) which avoids using phase angles, and fractal theory. But as shown in the above physical model, much ground needs yet to be covered between mathematical techniques and the results derived from the levitation reactor and the ESEM microreactor.

HETEROGENEITY/HOMOGENEITY IN PARTICLE- FLUID TWO-PHASE FLOW

(J. Li, D. Liu, G. Xu)

In 1946, when I was carrying our my dissertation research in fluidization, I was greatly fascinated by the different behaviors of particles while fluidized by a liquid and by a gas. Liquid/solid fluidization is quite homogeneous, and gas/solid fluidization is characterized by bubbling and slugging. The former was then designated "particulate" and the latter, "aggregative." Such distinction between particulate and aggregative fluidization has since commanded much attention, though relatively little has been discussed as to their common origin, or to their transition -- abrupt, gradual, or in what manner.

In later years, while developing new processes treating vast tonnages of low-grade ores, revelation from these two types of fluidization led me to realize that the conventional bubbling gas/solid fluidized bed consumes too much energy for the circulating gas and yet provides inadequate contact between gas and solids because of gas bypassing through bubbling. The solid particles need to be *dispersed discretely* as in particulate fluidization for liquid/solid systems. The answer was dilute-phase operation, which I adopted in most of the fluidized-bed metallurgical processes that I devised. A more basic question, however, was to look at fluidization of solid particles with a fluid having properties intermediate between those of a gas and of a liquid. I thought of the use of supercritical fluids, and in 1957 I collated data on fluids spanning the common liquids and gases, including gases under pressure.

In 1984, Jinghai Li came to me to study fast fluidization. I asked him to analyze the problem by resolving the particle-fluid system into three scales of interaction: a **micro** scale of the dimension of the individual particles, a **meso** scale of the dimension of the strands (or clusters) and a **macro** scale of the dimension of the equipment (**Figure 2-1**). A set of equations was written, but the constraints seemed to be one less than the variables specified. Jinghai believed that the phase structure of a particle-fluid system is an expression of its stability, which is determined by certain minimal energy of the system. He tried quite a number of formulations of the energy term, until he finally pinned down the *minimal energy for suspension and transport of the solids*.

Convergence in computation then posed another problem. When the computer began to yield smooth curves, we discovered that at some singular point the computed variables were discontinuous. This was soon understood to correspond to the common phenomenon of "choking." For solids with good fluidizing behavior, such as the Geldart Group A powders, choking is delayed to higher gas velocities. For normal liquid/solid systems, however, choking was found to be absent. Finally, we computed fluidization with supercritical CO_2, and found transitional behavior which varies continuously from G/S to L/S systems as pressure increases to near the critical point. We called the above model, the *Energy-Minimization Multi-Scale* model, or for short, the *EMMS* model.

Figure 2-2 compares the computed results for the FCC/air system against those for the glass/water system, to illustrate the disparate behaviors of G/S and L/S fluidization. The first two insets on the left-hand side show the change of voidage ε_f, ε_c and ε (dilute-, dense-phase and average, respectively) and cluster-phase fraction f for the FCC/air system. In the corresponding insets for the L/S system to the right, however, the three voidages ε_f, ε_c and ε are identical, and the cluster-phase fraction f is zero, indicating the absence of clusters throughout the velocity range of U_g, that is, fluidization is homogeneous.

variable, and under the control of this feed back loop, the chamber length L is maintained at an optimum resonant value and particles are levitated stably during the course of medium changes. **Figure 1-2** shows the heating, temperature measurement and image sampling system. The heating source is a CO_2 laser. The particle is irradiated and its temperature is measured by an infrared thermometer. Based on the error of the temperature signal, a microcomputer-based digital PID controller generates a control signal to vary the laser power required to maintain the particle at the desired temperature.

Chalk, plastics, glass and aluminum particles in the size range of 3 to 5 mm, as well as a 4-mm steel sphere have been successfully levitated in the apparatus. The ability of radial and vertical focusing was proved by the measured sound pressure distribution in the resonance chamber, as shown in **Figure 1-3,** for axial sound pressure distribution in the upper part of the chamber at ambient temperature with a particle levitated at the lowest sound pressure node. The distance between the adjacent pressure nodes was found approximately to be half of the calculated wavelength $\lambda_{0,1}$ for a (0,1) normal mode standing wave, which is the desired mode for providing radial focusing in the chamber.

For a levitated droplet of NH_4Cl solution, nascent crystals could be seen growing inside the droplet while crust formation proceeds simultaneously. Also evident are whisker/dendrite growths outside the crust extending into free space.

On an even finer scale, for what the human eye cannot discern and differentiate, the surface texture of the particle is often left unaccounted for. However, different individual microstructure of the same materials may induce diverse behaviors for the reacting particle. Due to its outstanding technological importance and extensive prior studies, the oxidation of iron was chosen as a model system for illustrating the significance of morphological changes at the surface. We shall describe experiments using *environmental scanning electron microscopy* (ESEM), in which specimens could be examined directly and continuously in a controlled reacting gas environment.

The KYKY 1500 ESEM, which we built in Beijing as shown in **Figure 1-4**, features a three-step vacuum system, a newly designed detector and a hot stage (the microreactor), with its gas supply system, graphics system and external temperature control system, all tailored specifically for dynamic and *in situ* observation and video recording in the microreactor. The specimens used in the present work were cylinders of 99.98 wt% electroformed iron, 2.4 mm in diameter, with polished surface. A VIDAS-25 graphics system, linked to the ESEM, sequentially recorded and stored the experimental data. Some specimens oxidized in the ESEM were further examined by using post-oxidation techniques, such as FESEM (AMRAY 1910 FE), petrographic analysis and Auger energy spectroscopy (AES PHI-610), for identifying and characterizing the oxidation products.

Three sets of experimental conditions were chosen to observe the different formation processes for different oxide grains of iron. In the **first** set of conditions, carried out at 500° C, argon was first introduced into the specimen chamber at about 200 Pa, until the desired temperature was reached and stabilized. Then air was mixed into the argon stream to an oxygen partial pressure P_O=3.2 Pa. **Figure 1-5** shows the successive changes at the surface, until finally new nuclei became whiskers. The **second** set of experiments was performed at 700°C at P_O=44 Pa. **Figure 1-6** shows that successive layers of particulate oxide grains formed from the metal substrate, which finally became whiskers, before eventual agglomeration. The **third** set of experiments was carried out at 600°C with programmed gas entry. The specimen was first heated with air with P_O=200 Pa, to form an initial oxide layer. When the desired temperature had been reached, argon was supplied to substitute air, with a residual $P_O=8.5 \times 10^{-4}$ Pa. The micrographs in **Figure 1-7** show a different process for iron oxide growth, resulting in relatively large rectangular grains which slowly changed to hexagonal grains.

The above three sets of experiments show that when oxidation was carried out under similar oxygen partial pressures but at different temperatures, the iron oxide products are totally different: thin, flat, leaf-like whiskers at 500°C (Figure 3(f)); agglomerated whiskers at 700°C (Figure 4(f)); rectangular and hexagonal grains at 600°C (Figure 7(f)). These oxides of different morphologies imply different growth mechanisms and reaction kinetics, thus calling for different modeling techniques. **Figure 1-8** presents a plausible physical model for the oxidation of iron on the basis of the ESEM observations described above. Next to the Fe surface is a thin layer of nucleation consisting of a

Figure 2-3 shows the gradual transition of the homogeneous glass/water fluidization to the highly heterogeneous, or aggregative glass/air fluidization, as the particle/fluid density ratio ρ_p/ρ_f increases from water through ethyl ether, and carbon dioxide under different stages of decreasing pressure down from its critical condition, to atmospheric air. The appearance and gradual growth of the two-phase structure is evident in the order of the fluids listed.

While Figure 2-2 demonstrates from our modeling the *disparate* nature between G/S and L/S fluidization, Figure 2-3 shows *continuity* in particle-fluid behavior through properly selected intermediate fluids, thus reconciling through modeling the phenomenological discrimination between particulate and aggregative fluidization.

Such computation needs to be corroborated by experiments. In 1990, Dejin Liu, was given the task of experimental investigation of fluidizing solid particles with supercritical CO_2. His experiments were conducted in a stainless steel column, 26 mm i.d. by 2 m high, connected to a CO_2 circulating, heating and regulating system as shown in **Figure 2-4**. These were supplemented with additional experiments using liquids less viscous and much more viscous than water, in another L/S system with a column of similar dimensions. Voidage of the fluidized solid particles and their fluctuations were measured by means of special optical fiber probes located along the column height, with on-line data acquisition and processing. Nine kinds of solid particles were used, ranging in **density** from the lightest for silica gel to steel, and in **size** from the smallest for alumina to steel balls. Seventeen species of liquid were used, ranging in **density** from the lightest for CO_2 at ambient conditions through CO_2 at 9.4 MPa, n-hexane, water to 70% aqueous glycerol, and in **viscosity** from the least viscous for CO_2 at ambient conditions, through CO_2 at 9.4 MPa, n-hexane, water to 70% aqueous glycerol.

While the EMMS model establishes on broad principles the distinction as well as reconciliation between particulate and aggregative fluidization, Dejin's experiments scan the more **specific** behaviors of the fluidized systems in order to supply other more descriptive criteria. These behaviors fall into the following three categories.

Spatio-temporal Voidage Fluctuation

Figure 2-5 shows typical *fluctuating voidages* for fluidizing particles with CO_2 under pressure: sand with CO_2 at 0.1 MPa, ion exchange resin at 3 MPa, and FCC catalyst at 6 MPa, in the order of increasing homogeneity. The simplest statistical parameter, the departure of the local and instantaneous voidage ε_i from its average value ε is used, in the form of the standard deviation:

$$\sigma = \sqrt{\frac{1}{n}\sum_{n=1}^{n}(\varepsilon_i - \varepsilon)^2}$$

The most heterogeneous fluidization occurs in slugging, for which voidage alternates between a dilute phase with voidage approaching unity and a dense phase with voidage approaching that at minimum fluidization ε_{mf}, with their respective fractional occurrences of f and (1 - f). According to Dejin's analysis, the maximum value of $\sigma_{slugging}$ occurs at $f = 1/2$, from which $\sigma_{max} = \frac{1-\varepsilon_{mf}}{2}$ and $\varepsilon_{\sigma_{max}} = \frac{1+\varepsilon_{mf}}{2}$.

A relative measure, called *heterogeneity index* δ, can thus be defined:

$$\delta = \frac{\sigma}{\sigma_{max}} = \frac{2\sigma}{1-\varepsilon_{mf}}.$$

The range of variation of δ is from 0 to 1:

$$\underset{\text{max homogeneity}}{0} < \delta < \underset{\text{max heterogeneity}}{1}$$

Expansion of Fluidized Bed with Velocity

For the velocity range between U_{mf} and U_t, *bed expansion* can be described in a global sense by the area under the voidage-*versus*-velocity curve, as shown in **Figure 2-6**:

$$A_R = \int_{U_{mf}}^{U_t} \varepsilon\, dU$$

where, for particulate fluidization, $U = U_t\varepsilon^n$, substitution and integration give

$$A_P = \frac{n}{n+1} U_t \left[1 - \left(\varepsilon_{mf} \right)^{\frac{n+1}{n}} \right]$$

As fluidization becomes less homogeneous, particles aggregate and the bed expands less, resulting in a smaller area, $A_R < A_P$. This deviation of A_R from A_P can be taken as a measure of the *global nonideality* f_h of the fluid-particle system:

$$f_h = \frac{A_P - A_R}{A_P} = 1 - \frac{\int_{U_{mf}}^{U_t} \varepsilon \, dU}{\frac{n}{n+1} U_t \left[1 - \left(\varepsilon_{mf} \right)^{\frac{n+1}{n}} \right]}$$

The range for the variation of f_h is also from 0 to 1:

$$0 < f_h < 1$$

max homogeneity max heterogeneity

Figure 2-7 shows three sets of experimental results for the variation of *bed expansion* and of *local heterogeneity* with fluid velocity for three kinds of particles. The lower set is for silica gel, which is relatively light, showing that the bed expands almost linearly with fluid velocity for n-hexane and CO_2 at 9, 8 and 6 MPa, while the local heterogeneity index δ starts from a very low value of 0.025, increasing in the order of the fluids mentioned. In this set, with CO_2 under progressively decreasing pressures, from 4 MPa to 0.1 MPa, bed expansion becomes more and more difficult as particles aggregation becomes more pronounced, while the local heterogeneity increases in that order up to a high value of 0.7. The middle set is for ion exchange resin, which is denser, showing that linear bed expansion is even poorer, and that the local heterogeneity index δ starts from a much higher value of 0.07. The upper set is for the heaviest particles tested, steel balls, showing that only aqueous glycerol solutions can maintain linear bed expansion, and even with CO_2 at 5 MPa, the local heterogeneity index is as high as 0.9.

Role of Particle and Fluid Properties

The choice of the dimensionless numbers involving *particle and fluid properties* to demarcate particulate from aggregative fluidization depends greatly on how well they fit experimental data. Dejin proposed what he called the *discrimination number:*

$$Dn = \left(\frac{Ar}{Re_{mf}} \right) \left(\frac{\rho_p - \rho_f}{\rho_f} \right)$$

Figure 2-8 shows the interrelationship between δ, f_h and Dn. Though they are well correlated, they belong, nevertheless, to totally different behaviors:

- δ *local heterogeneity* for spatio-temporal *fluctuation of voidage*
- f_h *global nonideality* for suppressed *bed expansion*
- ***Dn*** *discriminating* the contributing influences of *particle and fluid properties*

These criteria, therefore, represent but different quantified aspects of the same phenomena, each giving its own quantitative measure as to how far a particle-fluid system is removed from aggregative fluidization and how close it is to particulate fluidization.

As originally formulated, the EMMS model was in the form of an optimization problem. Solution depended on the use of the GRG2 (General Reduced Gradient) program, which was time consuming and often did not converge easily. To facilitate the application of the EMMS model to engineering problems, attempts were made for simpler solutions. Guangwen Xu (1997) devised an analytical approach which reduces the computation time from *minutes* and *hours* to *seconds*.

Fifty years ago, as a student, I studied fluidization and observed the liquid/solid pairs that fluidize particulately and the gas/solid pairs that fluidize aggregatively. Not only out of curiosity to pursue the unknown, but also driven by practical motives for developing new processes and improving existing processes, I have been, for the better part of my life, looking for the link between the two. The answer has come through the efforts of three generations of investigators ---- my teacher, myself and my two students.

Through such a knowledge of the common basis of particulate *vis-a-vis* aggregative fluidization, we may well be able to better fluidize a solid, be that with a liquid or with a gas. Could we, for instance, possibly "particulatize" a gas/solid system in the direction of a liquid/solid system, for instance, in devising a feed/transport/injection system for powdered coal,

which operates as smoothly as coal-water-mixture yet without the loss of gasification or combustion efficiency due to the presence of the carrying fluid, water. Or could we think of some way of increasing the throughput of liquid/solid fluidization, e.g., fluidized leaching and/or washing, by the incorporation of small quantities of ferromagnetic micro particles for operation in some kind of a magnetic environment, strategically emplaced in the processing vessel, with alternating or even electrically moving field. We may have exhausted our present arsenal of concepts, and need to create new weaponry of ideas.

IMPROVEMENT OF G/L CONTACTING WITH FLUIDIZED SOLIDS

(X. Ma, F. Ouyang, Y. Wu, L. Cheng)

Magnetofluidization was first used in the containment of iron-based catalyst particles in G/S fluid-bed reactors, for instance, in ammonia synthesis and water-gas shift reaction. The magnetic filed is capable of holding back the ferromagnetic catalyst particles against an upflowing gas stream. Applied to G/L/S systems, magnetofluidization can disintegrate gas bubbles. Whereas bubbles in G/L/S systems are quite different from bubbles for G/S systems, they share the common feature that the parallel lines of a uniform magnetic field are flexed by the presence of a void, in which there are no ferromagnetic particles, and thus create a magnetic tension oriented toward the center of the bubble, forcing the ferromagnetic particles to penetrate and fall into the bubble.

Experiments for G/L/S magnetofluidization were carried out in a two-dimensional bed as shown in **Figure 3-1**, 150 x 10 x 1000 in inside dimension. Iron granules, 0.09 to 0.37 mm in diameter, were fluidized with water doped with a common detergent to alter its surface tension. Air was injected via a solenoid valve through a 3-mm nozzle closely above the liquid distributor, to generate single bubbles. A horse-shoe electromagnet supplied a horizontal magnetic field through the frontal surface of the 2-D bed. **Figure 3-2** shows the bubble detector, which consists of a lower horizontal row of 29 photocells deployed equidistantly at 5-mm intervals, and a single horizontally movable upper probe, located 18 mm above the lower row. Illumination from the opposite side of the 2-D bed sent parallel rays through the bed front towards the bubble detector. Signals from the 30 photocells were sent to a computer for on-line processing. **Figure 3-3** shows a computer printout of the bubble pattern. **Figure 3-4** shows a series of pictures of bubble behavior under different magnetic field strengths. Without any magnetic field, H = 0 Oe, Figure 3-4a shows a large single bubble, about 9 cm in diameter, from the injected air pulse. With increasing magnetic field strength, $0 < H < 80$ Oe, Figures 3-4b and 3-4c show the big bubble breaks up into progressively smaller bubbles. Here, particles can be seen showering from the roof of the bubble to cleave it into smaller fragments.

The bubble roof is subject to both the magnetic force of particle penetration and the gravity force of the particles from above, and therefore becomes the weak point of fracture. Through formulation of the magnetic, interfacial-tension, pressure, gravitational and drag forces, an expression has been derived for computing the maximum stable bubble size. **Figure 3-5** shows the effect of magnetic field strength on *bubble diameter* with changing liquid and gas flow rates, particle diameter and gas-liquid interfacial tension. The points in this figure are experimental and the curves are computed. Similarly, **Figure 3-6** shows the effect of magnetic field strength on *bubble velocity* with the same set of changing parameters.

Figure 3-7 shows a magnetofluidized G/L/S ethanol bioreactor, which employs a magnetic distributor-downcomer consisting of an iron mesh surrounded by a collar-type magnetizing coil. The solid particles are immobilized yeast on alginate beads with molded-in magnetite powder. These ferromagnetic particles, when placed in the magnetic field, prevent their being carried upward as a scum by the CO_2 bubbles derived from fermentation which adhere to the particles. When the coil is magnetized, a nonuniform magnetic field is created above and below the distributor, resulting in the formation of all the three regimes of magnetofluidized L/S systems: particulate, chain and magnetically condensed, ordered as above according to their proximity to the magnetic distributor-downcomer.

Magnetofluidization is fairly well provided with basics studies and can be considered a propitious area for new innovative techniques.

FLUIDIZATION OF PARTICLES WITH APPRECIABLE INTER-PARTICLE FORCES

(Z. Wang, H. Li)

In the offing there will be more fluidization techniques dealing with or making use of inter-particle forces. These range from ash-agglomerating coal gasification, the preparation and processing of ultrafine particles, to granulation of powders, including the preparation of detergents coated with proteinase and the making of Chinese micro-pill herb medicines which are easier to swallow than mega-sized capsules. Such techniques constitute a class in its own, involving somewhat common mechanisms and calling for somewhat generic tools for analysis and design.

Take as an example, the study of fine particles. Fine particles are understood to be particles fine enough to show appreciable cohesion between particles and adhesion between particles and any surface in contact. The behavior of fine particles when fluidized is highly unpredictable and therefore experimental results would be more *representative* than *reproducible*. To insure a higher degree of representativeness, different types of experiments are performed on samples to look for mutual congruence: bed expansion upon fluidization, bed collapsing test, measurement of cohesiveness among particles, dynamic video recording of fluidization behavior followed by image analysis, measurement of porosity of bulk solids. The results of these individual tests are collated to sharpen the overall representativeness of the fine particle behaviors.

Figure 4-1 shows the experimental fluidized bed which measures 33 mm in inside diameter and 1000 mm in height. Bed collapsing test was performed by instantly cutting off the fluidizing air by a solenoid valve, following the descending bed surface by a Sony handycam camera and processing the collapsing curves with a PC computer. Fine particles used were goethite, titanium dioxide, talc, alumina, nickel, magnetite, zeolite, aerogel, etc., ranging in size from 0.01 to 18.1 μm and in density from 100 to 8600 kg/m^3.

Figure 4-2 shows that goethite particles, for instance, initially form a plug with a high pressure drop of 32 mm H_2O, much greater than the apparent weight of the particles. The plug splits and the bed channels at U=0.02 m/s, whereby the pressure suddenly drops to a low value of 3.5 mm H_2O. When the gas velocity is increased to 0.04 m/s, the pressure drop rises abruptly to 30 mm H_2O, and the bed disrupts itself and the particles are fluidized, and thereafter the bed expands with further increase in gas velocity from 180 to 345 mm, while the pressure drop remains essentially the same.

As a whole, the process of fluidizing fine particles usually involves plugging, channeling, disrupting and agglomerating, and their combinations, each highly specific and characteristic of the particles being dealt with. Beds of fine particles could generally be disrupted suddenly at some characteristic gas velocity, called the disrupting velocity, $U_{disrupt}$.

Bed collapsing behavior of fine particles generally falls into two classes. In the first case, for particles with very small bed expansion and serious channeling, their beds hardly collapse. The second class refers to particles with some appreciable expansion ratio, demonstrating the three-stage collapsing characteristics of Geldart group A particles, such as for goethite as shown in Figure 4-2. For these particles, different sizes of agglomerates of fine particles are formed, and often the hindered sedimentation stage is long.

Experiments showed that when fine particles agglomerate during fluidization, the larger agglomerates often gravitate to the bottom sometimes forming a fixed bed, the medium agglomerates are fluidized in the middle, and there is a dilute-phase at the top consisting of small agglomerates and discrete, unassociated particles. The agglomerates were photographed at different bed heights and the agglomerate sizes were measured to give the agglomerate size distribution shown in **Figure 4-3**.

The height of the agglomerate layer first increases rapidly, and then, as larger agglomerates are broken into smaller ones and elutriated out, the agglomerate layer decreases. When the elutriated agglomerates are collected and recycled repeatedly into the bed, the average size of the agglomerates would decrease and become more or less constant. These final agglomerates would fluidize homogeneously. This phenomenon suggests the use of circulating fluidized bed to achieve better fluidization of fine particles through this process of *equilibrium agglomeration.*

Fine particles tend to form globular agglomerates when kept in a heap, stored in a vessel, or while being transferred, that is, whenever relative motion exists between particles. These agglomerates, called *natural agglomerates*, are generally light and friable in structure, and possess relative close size ranges. When

fluidized, the natural agglomerates undergo reorganization, or are fragmented into smaller agglomerates or even discrete particles, which reform afresh new agglomerates, the *fluidized agglomerates.*

Analysis of experimental results showed that

- The stability of natural agglomerates increases with decrease of particle size.
- Better fluidization results for multi-sized agglomerates.
- Low-density agglomerates fluidize better.
- The larger agglomerates at the bottom of a fluidized bed are usually composed of smaller parent individual particles, while the smaller agglomerates further up in the bed consist of larger members of the parent discrete particles.
- Channeling and slugging always take place for fine particles, and channels can form either directly from the discrete fine particles or from their agglomerates.

The fluidizing behavior of fine particle agglomerates may be compared to that of normal discrete particles as shown in **Figure 4-4**. The top line shows the normal fluidization of discrete noncohesive particles, spanning the velocity range from minimum fluidization U_{mf} to particle transport U_t. The bottom line shows the worst case for unfluidizable fine particles which channel or rat-hole for the entire velocity range from computed particle minimum fluidization at U_{mf} to transport of the unfluidized particles as a single agglomerate at $U_{transport}$. Then, from the upper left corner of the rectangle a line is drawn to the lower right corner to represent the locus of the disruptive velocity $U_{disrupt}$. For any sample of particles which channel at low velocity and fluidize with agglomerate formation at higher velocity, there exists a horizontal line starting from some point C, between the top and bottom lines, to intersect this $U_{disrupt}$ locus at a point equal to its disruptive velocity, to demarcate the channelling/rat-holing behavior toward the left from the agglomerate fluidizing behavior toward the right. The lower is this C-line, the greater is the fractional velocity range for channelling/rat-holing. Thus, if we graduate the ordinate between zero and unity to represent an arbitrary scale of relative cohesiveness, RC, then the area of the lefthand-side triangle above the C-line will represent the departure of the fine particles chosen from discrete particles, and the full range for RC will represent all the intermediate behaviors between zero for normal fluidization of non-cohesive particles and unity for unfluidizable fine particles:

$$0 < (RC)^2 < 1$$

normal fluidization -- channelling/rat-holing
unfluidizable non-cohesive particles
(followed by fine particles agglomerate fluidization)

Of course, the $U_{disrupt}$-locus should be experimentally determined, rather than expressed as a straight line as shown, and the departure from normal fluidization should be evaluated by integration along the U-axis.

The multi-phase nature of fluidization has provided us with a rich spectrum of challenging problems. Heterogeneity/homogeneity has been an outstanding problem for decades. We have proposed a solution, though far from being perfect. The morphology and texture studies are aimed at better modeling of solid-state changes. They call for some knowledge of non-chemical-engineering areas, viz., acoustics and microscopy. Improvement of G/L contacting with magnetofluidization is focused on the utilization of readily available basic studies. Current interest in ultrafine particle fluidization is being foreseen as an extending field to allied processes dealing with or making use of inter-particle forces. It is hard to generalize as to how to identify problems related to the multi-phase nature of fluidization. For one thing, they are usually situated at the intersections between technologies, sciences and even professions. Neither it is easy to generalize on the solution of these problems. Often they call for some knowledge of neighboring science or technology. As a whole, the multi-phase nature of fluidization calls upon the chemical engineer to know more about other technologies and to be prepared to be apprentice of other disciplines in science and technology.

The past half a century or so has seen tremendous growths and accomplishments in fluidization. But we can further benefit ourselves from fresh fertile areas of endeavors. Isolated, every new concept or innovative device/process is a step-change of breakthrough, but, taken as a whole, progress stands for continual integration of the inheritance of the accepted and imagination of the unexpected. I am sure there will be many such step-change breakthroughs in this symposium, and I sincerely wish you success in this meeting.

PRINCIPAL REFERENCES

1. Cao, Z., Liu, S., Li, Z., and Gong, M., Development of an Acoustic Levitation Reactor, *Powd. Technol.*, 69, 125-131 (1992)
2. Cao, Z., Liu, S., and Li, Z., Acoustic Levitation Reactor, *14th Intern. Congr. Acoustics*, Beijing, 1992
3. Cao, Z., Liu, S., Li, Z., Diao, Y., Pan, D., and Luo, B., The Design and Control of an Acoustic Levitation Reactor, *Chem. Reaction Eng. & Technol.*, 11(2), 120-127 (1995)
4. Cao, Z., Li, Z., and Liu, S., Resonance Tracking System for Acoustic Levitation Apparatus, Chinese Pat. Appl. CN 1056176 91103537.0 (Nov. 13, 1991)
5. Kwauk, M., Ma, X., Ouyang, F., Wu, Y., Weng, D., and Cheng, L., Magnetofluidized G/L/S Systems, *Chem. Eng. Sci.*, 47(13/14), 3467- 3474 (1992)
6. Li, J., and Kwauk, M., "Particle-Fluid Two-Phase Flow – the Energy-Minimization Multi-Scale Method," Metallurgical Industry Press, China, 204 pp (1994)
7. Liu, D., Kwauk, M., and Li, H., Aggregative and Particulate Fluidization – the Two Extremes of a Continuous Spectrum, *Chem. Eng. Sci.*, 51(17), 4045-4063 (1996)
8. Ma, X., Pure Sine Descriptors for Particle Shape Analysis, Particuology '88 (*Proc. Trilat. Symp. Particuology*, Sept. 5-9, 1988), p. 7-12
9. Ma, X., and Kwauk, M., Particulate Fluidization of Ferromagnetic Particles in Uniform Magnetic Field, *CREEM Seminar* (Chem. Reaction Eng. In Extractive Metall.), Beijing, May 1985, p. 248-267; *Pacific Reg. Meet. of Fine Particle Soc. (U.S.A.)*, Honolulu, Hawaii, Aug. 1-5, 1983, Proc., ed. T. Ariman, p. 117
10. Ouyang, F., Wu, Y., Guo C., and Kwauk, M., Fluidization under External Forces (1) Magnetized Fluidization, *J. Chem. Ind. Eng. (China)*, 5(2), 206-222 (1990)
11. Shao, M., Li, H., and Kwauk, M., Morphological Changes of Oxide Grains during Oxidation of Pure Iron in an Environmental Scanning Electron Microscope, *Particle & Particle Characterization*, 14(1), 35-40 (1997)
12. Wang, Z., Kwauk, M., and Li, H., Fluidization of Fine Particles, *Chem.Eng. Sci.*, in press
13. Wilhelm, R. H., and Kwauk, M., Fluidization of Solids Particles, *Chem. Eng. Prog.*, 44, 201 (1948)
14. Xu, G., and Li, J., Analytical Solution of the Energy-Minimization Multi-Scale Model for Particle-Fluid Two-Phase Flow, *Chem. Eng. Sci.*, in press

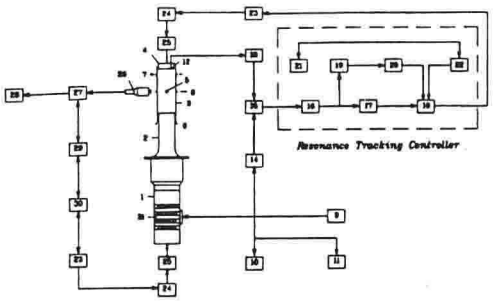

Figure 1-1. Acoustic levitation reactor with its resonance tracking and particle position control systems

1. Ultrasonic transducer, 2. Stepped horn, 3. Resonance chamber, 4. Reflector, 5. Levitated particle, 6. Gas inlet, 7. Gas outlet, 8. Windows, 9. Ultrasonic signal generator, 10. Frequency counter, 11. Oscilloscope, 12. Condencer microphone, 13. Microphone amplifier, 14. Measurement amplifier, 15. Lock-in amplifier, 16. Deviation amplifier, 17. Window comparator, 18. Gate circuit, 19. Absolute value circuit, 20. Voltage controlled oscillator, 21. Position indicator, 22. Overshoot alarm, 23. Stepping motor power supply and controller, 24. Stepping motor, 25. Drive mechanism, 26. CCD camera, 27. Videographic system board, 28. Color video monitor, 29. Microcomputer, 30. Data logger, 31. Thermocouple.

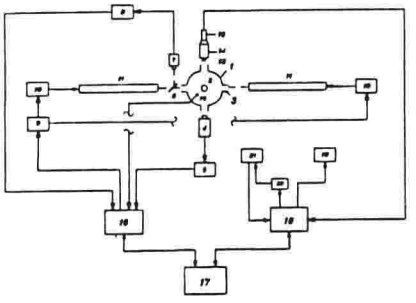

Figure 1-2 Heating and temperature control and image sampling subsystems

1. Resonance chamber, 2. Levitated particle, 3. Windows, 4. Infrared detector, 5. Indicator and transducer of infrared thermometer, 6. CO_2 laser beam splitter, 7. Detector of laser power meter, 8. Indicator and transducer of laser power meter, 9. Trigger-selector switch, 10. Neon bulb transformer, 11. CW CO_2 laser, 12. Thermocouple, 13. Fixed-focus lens, 14. Zoom lens, 15. CCD camera, 16. Data logger, 17. Microcomputer, 18. Videographic system board, 19. Color video monitor, 20. Color TV encoder, 21. Video recorder.

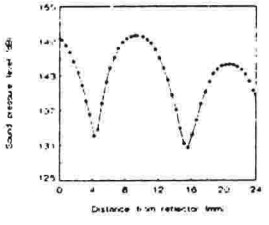

Figure 1-3. Axial pressure distribution above particle levitated at lowest sound pressure node

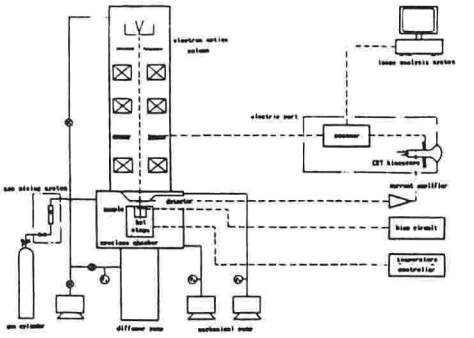

Figure 1-4. Diagrammatic sketch of the KYKY 1500 ESEM with hot stage

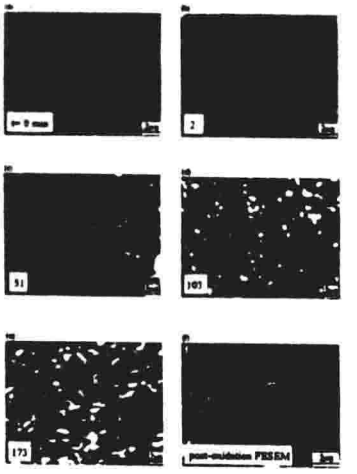

Evolution of iron oxidation at 500°C and P_{H_2O} = 3.2 Pa in the ESEM. (a) Unoxidized surface at 14°C. (b) t = 2 min. (c) t = 51 min. (d) t = 103 min; (e) t = 173 min (f) oxide whisker as shown by the AMRAY 1910 FESEM at 14°C, same conditions as (e).

Figure 1-5 Oxidation of Fe at 500° and P_O=3.2 Pa *to Whiskers*

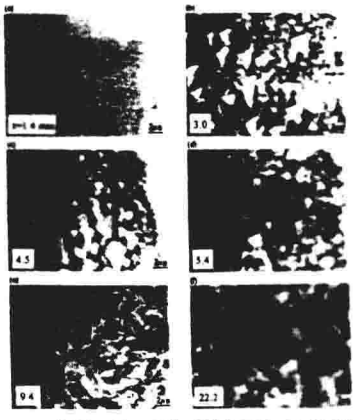

Evolution of iron oxidation at 700°C and P_{H_2O} = 44 Pa in the ESEM. (a) t = 1.4 min, (b) t = 3.0 min, (c) t = 4.5 min, (d) t = 5.4 min, (e) t = 9.4 min; (f) t = 22.2 min.

Figure 1-6. Oxidation of Fe at 700° and P_{H_2O}=44 Pa *to Whiskers and Whisker Agglomerates*

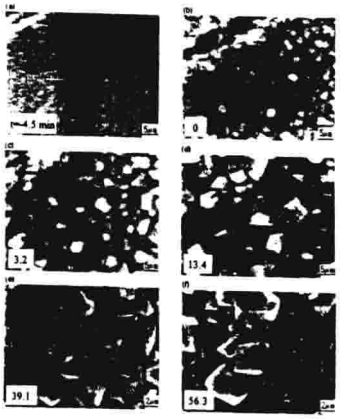

Evolution of iron oxidation at 600°C and P_{O2} from atmospheric air to $8.5 \cdot 10^{-4}$ Pa in ESEM. (a) t = −4.5 min (547°C); (b) t = 0 min; (c) t = 3.2 min; (d) t = 13.4 min; (e) t = 39.1 min; (f) t = 56.3 min.

Figure 1-7. Oxidation of Fe at 600° and P_{O2}=200/8.5x10^{-4} Pa *to Rectangular and Hexagonal Grains.*

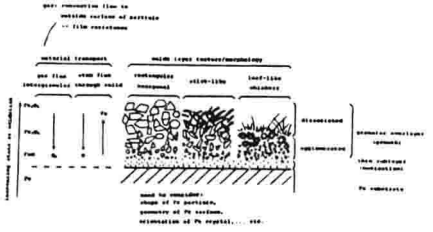

Figure 1-8. Plausible physical model for oxidation of Fe based on ESEM observations

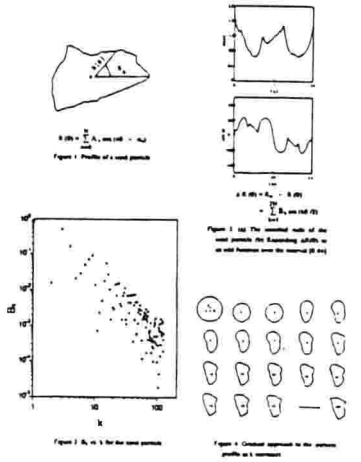

Figure 1-9. Fourier wave vectors for particle designation

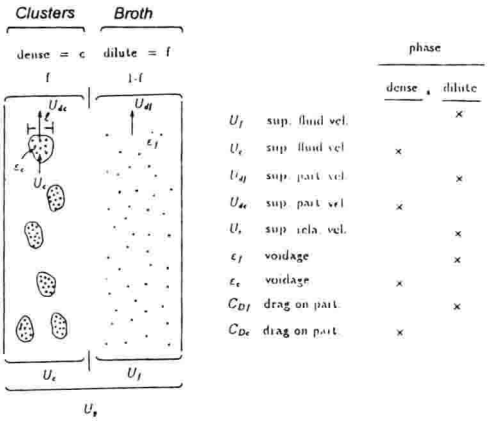

Figure 2-1. Physical Model for Multi-Scale Modeling of Particle-Fluid System

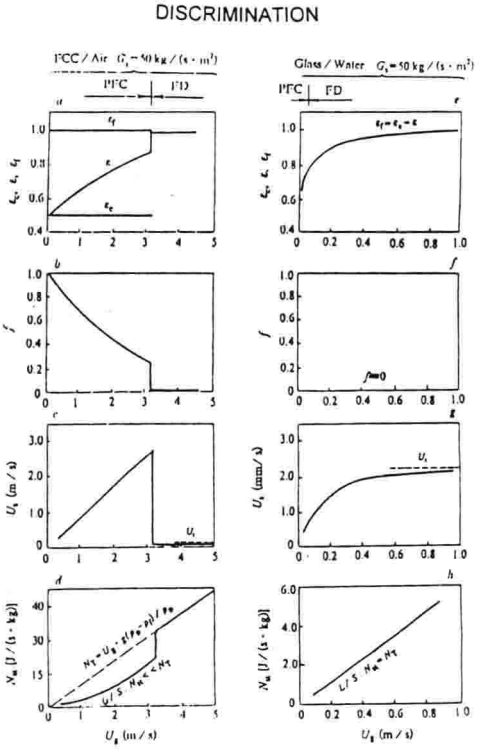

Figure 2-2. Differences between G/S and L/S Systems